Monthly Notices of the ROYAL ASTRONOMICAL SOCIETY

MNRAS **465,** 834–842 (2017) doi:10.1093/mnras/stw2845
Advance Access publication 2016 November 4

# The ALMA early science view of FUor/EXor objects – I. Through the looking-glass of V2775 Ori

Alice Zurlo,[1,2,3]★ Lucas A. Cieza,[2,3] Jonathan P. Williams,[4] Hector Canovas,[5,3] Sebastian Perez,[1,3] Antonio Hales,[6] Koraljka Mužić,[2] David A. Principe,[2,3] Dary Ruíz-Rodríguez,[7] John Tobin,[8] Yichen Zhang,[1] Zhaohuan Zhu,[9] Simon Casassus[1,3] and Jose L. Prieto[2]

[1]*Universidad de Chile, Camino el Observatorio 1515, Santiago, Chile*
[2]*Núcleo de Astronomía, Facultad de Ingeniería, Universidad Diego Portales, Av. Ejercito 441, Santiago, Chile*
[3]*Millenium Nucleus 'Protoplanetary Disks in ALMA Early Science', Universidad de Valparáiso, Av. Gran Bretaña 8330015 Valparáiso, Chile*
[4]*Institute for Astronomy, University of Hawaii at Manoa, Honolulu, HI, 96822, USA*
[5]*Departamento de Física Teórica, Universidad Autónoma de Madrid, Cantoblanco, E-28049 Madrid, Spain*
[6]*Atacama Large Millimeter/Submillimeter Array, Joint ALMA Observatory, Alonso de Córdova 3107, Vitacura 763-0355, Santiago, Chile*
[7]*Research School of Astronomy and Astrophysics, Australian National University, Canberra, ACT 2611, Australia*
[8]*Veni Fellow, Leiden Observatory, Leiden University, PO Box 9513, NL-2300-RA Leiden, the Netherlands*
[9]*Department of Astrophysical Sciences, Princeton University, Princeton, NJ 08544, USA*

Accepted 2016 November 2. Received 2016 November 2; in original form 2016 July 10

## ABSTRACT

As part of an Atacama Large Millimeter/submillimiter Array (ALMA) survey to study the origin of episodic accretion in young eruptive variables, we have observed the circum-stellar environment of the star V2775 Ori. This object is a very young, pre-main sequence object which displays a large amplitude outburst characteristic of the FUor class. We present Cycle-2 band 6 observations of V2775 Ori with a continuum and CO (2–1) isotopologue resolution of 0.25 arcsec (103 au). We report the detection of a marginally resolved circum-stellar disc in the ALMA continuum with an integrated flux of 106 ± 2 mJy, characteristic radius of ∼30 au, inclination of $14.0^{+7.8}_{-14.5}$ deg and is oriented nearly face-on with respect to the plane of the sky. The $^{12}$CO emission is separated into distinct blue and redshifted regions that appear to be rings or shells of expanding material from quasi-episodic outbursts. The system is oriented in such a way that the disc is seen through the outflow remnant of V2775 Ori, which has an axis along our line of sight. The $^{13}$CO emission displays similar structure to that of the $^{12}$CO, while the C$^{18}$O line emission is very weak. We calculated the expansion velocities of the low- and medium-density material with respect to the disc to be of −2.85 (blue), 4.4 (red) and −1.35 and 1.15 km s$^{-1}$ (for blue and red) and we derived the mass, momentum and kinetic energy of the expanding gas. The outflow has an hourglass shape where the cavities are not seen. We interpret the shapes that the gas traces as cavities excavated by an ancient outflow. We report a detection of line emission from the circumstellar disc and derive a lower limit of the gas mass of 3 $M_{\rm Jup}$.

**Key words:** methods: data analysis – techniques: interferometric – stars: individual: V2775 Ori – stars: jets – stars: protostars.

## 1 INTRODUCTION

FU Orionis stars (FUors) are variable, pre-main-sequence low-mass stars that display brightness variations on a very short time-scale (less than one year) (Herbig 1966). Their brightness can increase by 3–6 mag at optical wavelengths during the course of a few months and remain bright for decades, a phenomenon called 'outburst'. According to the episodic accretion scenario (Hartmann & Kenyon 1996; Audard et al. 2014), most young stars are expected to experience these extreme luminosity outbursts during their early evolution.

The mechanism producing these sudden mass-accretion events, and thus the origin of these outbursts, is still poorly understood and currently there are several theories proposed: disc fragmentation (Vorobyov & Basu 2005; Zhu et al. 2012), thermal instability (Bell & Lin 1994), coupling of gravitational and magneto-rotational

★ E-mail: alice.zurlo.astro@gmail.com

instability (Armitage, Livio & Pringle 2001; Zhu et al. 2009) and tidal interaction between the disc and a companion (Lodato & Clarke 2004; Bonnell & Bastien 1992). During their ourbursts, the bolometric luminosity of the FUor type stars is 50–500 $L_{\odot}$, and the accretion rate is between $10^{-6}$ and $10^{-4}$ $M_{\odot}$ $yr^{-1}$ (Audard et al. 2014). Over the full duration of an outburst, the star may accrete ∼0.01 $M_{\odot}$ of material, roughly the mass of a typical T Tauri disc (Andrews & Williams 2005). During this phase, FUors show F–G supergiant optical spectra but with broader lines than those of T Tauri stars and K–M supergiant near-infrared spectra, showing CO overtone absorption (Zhu et al. 2009). The Fe I, Li I, Ca I, and CO lines are double peaked and show broadening, as expected for a rotating disc kinematic (Hartmann & Kenyon 1996). Single dish millimeter observations indicate that FUors look more similar to Class I protostars rather than Class II stars (Sandell & Weintraub 2001). However, interferometric data with enhanced angular resolution and sensitivity are required to demonstrate this (e.g. Hales et al. 2015). The outflows of these objects are driven by repeated outbursts with peak mass-loss rate of $10^{-5}$ $M_{\odot}$ $yr^{-1}$ (Evans et al. 1994); the dusty environment of FUors stars shows a core/envelope region structure, in contrast to Herbig Ae/Be (HAEBE) stars which show a core structure (Henning et al. 1998); and to well characterize the structure of FUors, it is necessary to use interferometric (opposed to single dish) observations that are necessary to characterize the circum-stellar structure and environment of FUor objects (Kóspál 2011).

The FUor type star V2775 Ori was first identified by Caratti o Garatti et al. (2011) and is located in the Orion molecular clouds, near the southern edge of the L1641 region, at a distance of 414 ± 7 pc (Menten et al. 2007). Caratti o Garatti et al. (2011) describe it as a young stellar object (YSO) with characteristics of both FUors and EXors (from the prototype FU Ori and EX Lup, respectively). EXors are pre-main-sequence stars that display shorter time-scale outbursts than the FUors. The spectrum of V2775 Ori shows a featureless continuum, with strong CO bands and $H_2O$ broad-band absorption (typical of the FUors) and Br $\gamma$ line in emission (as the EXors). Caratti o Garatti et al. (2011) derived an effective temperature $T_{\rm eff}$ = 3200 K, mass $M_{\star}$= 0.25 $M_{\odot}$ and an accretion rate of $\dot{M}$= 1.2 × $10^{-6}$ $M_{\odot}$ $yr^{-1}$. This makes it one of the lowest mass YSOs with a strong outburst discovered so far. The outburst of this object began in between 2005 April and 2007 March (Fischer et al. 2012).

Fischer et al. (2012) found that the disc accretion rate of V2775 Ori during the ourburst increased from ∼2 × $10^{-6}$ $M_{\odot}$ $yr^{-1}$ to ∼$10^{-5}$ $M_{\odot}$ $yr^{-1}$, about an order of magnitude less than the canonical value for the FUors ($10^{-4}$ $M_{\odot}$ $yr^{-1}$; Hartmann & Kenyon 1996). V2775 Ori is the least luminous documented FUor outburster with a protostellar envelope (L = 28 $L_{\odot}$). They modelled the source and obtained a mass for the star of $M_{\star}$= 0.5 $M_{\odot}$, which is consistent with the mass obtained in Gramajo, Rodón & Gómez (2014). However, they argue that the value of the mass is more likely around 0.24 $M_{\odot}$, more consistent with the value given by Caratti o Garatti et al. (2011). Gramajo et al. (2014) estimated that the temperature of the star before and after the outburst (5600 and 6800 K, respectively) is significantly higher than the temperatures calculated by Caratti o Garatti et al. (2011) and Fischer et al. (2012), about 3200–4000 K. They obtained an increase in the disc mass-accretion rate of one order of magnitude larger than what Fischer et al. (2012) derived. Gramajo et al. (2014) concluded that before the outburst, V2775 Ori was a Class I object and during the outburst, it is in the late stages of this class.

In this paper, we present the first ALMA observations of the FUor object V2775 Ori. This object was observed as part of a survey of eight FUor and EXor targets in Orion (PI: Cieza, project code: 2013.1.00710.S). The aim of this project is to investigate the origin of episodic accretion and to compare and contrast the physical characteristics of FUor/EXors with those of classical T Tauri discs. Understanding the origin of disc episodic accretion, as well as its consequences over the disc structure, is crucial for both star and planet formation (see Cieza et al. 2016, and upcoming papers by Ruíz-Rodríguez et al. 2016; Principe et al., in preparation; Cieza et al., in preparation). The observations and data reduction are presented in Section 2, followed by the results in Section 3 and the discussion in Section 4. A summary is given in Section 5.

**Table 1.** Beam information of the final combined data set.

| | Continuum | $^{12}$CO | $^{13}$CO | C$^{18}$O |
|---|---|---|---|---|
| Major axis ( arcsec) | 0.25 | 0.35 | 0.37 | 0.37 |
| Minor axis ( arcsec) | 0.17 | 0.27 | 0.28 | 0.29 |
| Pos. angle (°) | − 89.09 | − 89.98 | 86.70 | 87.07 |

## 2 OBSERVATIONS AND DATA REDUCTION

### 2.1 ALMA data

V2775 Ori has been observed three times with ALMA during Cycle-2 in band 6, as part of the Orion FUor/EXor survey. Two of three observations took place on 2014 December and 2015 April 5. The precipitable water vapour (PWV) was 0.7 and 1.3 mm for the December and April observations, respectively. The configuration of ALMA for both observing runs was with 45 antennas (12-m of diameter) with baselines ranging from 14.6 to 348.5 m. In this array configuration, the maximum recoverable scale of the emission is 11.4 arcsec, which means that smooth emission at larger angular scales (e.g. from the molecular cloud or the envelope) could be missed by our observations. ALMA observations provided two spectral windows for the continuum, centred at 232.6 GHz and 218.0 GHz, 2 GHz wide, plus three narrow (59 MHz wide) bands: one centred on the $^{12}$CO(2–1, 230.5380 GHz) line (hereafter $^{12}$CO), the second centred on the $^{13}$CO (2–1, 220.3987 GHz) line and finally, one centred on the C$^{18}$O (2–1, 219.5603 GHz) line. The resolution of these data sets is ∼0.8 arcsec. The correlator setup was identical for all the observations. Ganymede and J0423-013 were used as flux calibrators, while the quasars J0538-4405 and J0607-0834 where observed for bandpass calibration. Observations of nearby phase calibrators (J0541-0541, J0532-0307 and/or J0529-0519) were alternated with the science target to calibrate the time-dependence variations of the complex gains.

The third and final observations were performed on 2015 August 30 with an array of 35 antennas and longer baselines of 42–1574 m. For these data, the resolution was higher with respect to the data from December and April, reaching ∼0.25 arcsec. The PWV during the observations was ∼1 mm.

The data from all three epochs were processed and combined into a single data set. The visibility data were reduced using the Common Astronomical Software Application (CASA v4.4) package (McMullin et al. 2007). First, we concatenated the lower and higher resolutions data. The images of the continuum and the gas line data cubes were created with the pipeline using the calibrated visibilities and the CLEAN routine of CASA. Continuum subtraction was performed in the visibility domain. The characteristics of the beam used in the final combined data set and analysis are detailed in Table 1. The rms in

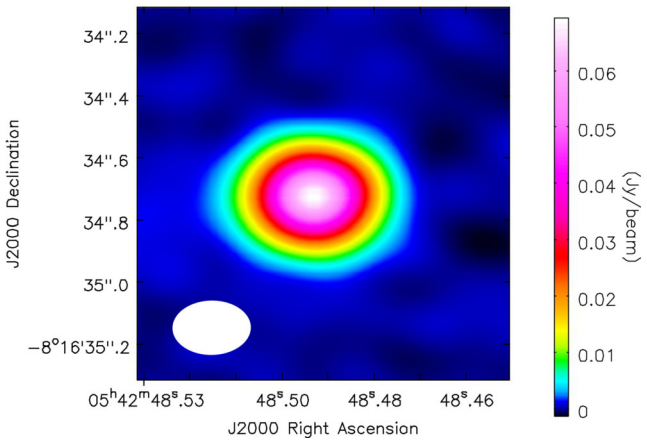


**Figure 1.** Image of the continuum emission of the FUor V2775 Ori. The beam size is ∼0.25 arcsec, shown on the lower-left corner of the image.

the final continuum and line data are 0.25 mJy beam$^{-1}$ and 15 mJy beam$^{-1}$ km s$^{-1}$, respectively.

## 3 RESULTS

### 3.1 Continuum emission

The image of the continuum of V2775 Ori is shown in Fig. 1, with an integrated flux 106 ± 11 mJy and a peak flux 69 ± 0.43 mJy beam$^{-1}$ (signal-to-noise ratio, SNR = 160). As the continuum image does not present any asymmetric structure, we performed a Gaussian two-dimensional fit with the CASA routine IMFIT and find that the dimensions of the disc, deconvolved from the beam, are 151.0 ± 3.6 mas (63 ± 2 au) for the major axis and 146.5 ± 3.7 mas (61 ± 2 au) for the minor axis. The position angle of the disc is 48° ± 35°. Assuming that the disc is circular, from the aspect ratio, we calculated that the disc is almost face-on with respect to the plane of the sky, with an inclination of $14.0^{+7.8}_{-14.5}$ deg. The centre of the disc is found in the sky location $\alpha_{2000} = 05^{h}42^{m}48^{s}.49$ and $\delta_{2000} = -8°16'34''.72$, slightly shifted from the ALMA phase centre. The infrared coordinates (Cutri et al. 2003) of the star perfectly match the ALMA coordinates apart from a small shift of 0.02 arcsec in the declination. A more detailed analysis and modelling of the continuum can be found in Cieza et al., in preparation.

### 3.2 $^{12}$CO moments

The $^{12}$CO line traces the outflow of the FUor star in the highest velocities, while the emission close to the system velocity may come from gas of the envelope or the disc around the central star. We assume that the system velocity corresponds to the velocity of the C$^{18}$O, which has faint emission in correspondence of the disc continuum emission. The velocity of the system is 3.1 ± 0.3 km s$^{-1}$. This value has been obtained fitting a Gaussian to the peak emission of the line.

We calculated the mean intensity of the molecular lines in a circular region centred on the continuum emission and with a diameter of 19 arcsec (∼7800 au), to include the whole emission from the gas, after a first determination of its extension with a map integrated along the velocity channels. The channel width used for this analysis is 0.25 km s$^{-1}$ and the rms is 14.46 mJy beam$^{-1}$ km s$^{-1}$. We find three peaks in the $^{12}$CO line mean flux (inside the 19 arcsec region) versus velocity profile, as shown in Fig. 2. We calculated the velocities-integrated intensity (moment 0) of the gas line for three different parts, corresponding to the three peaks: the 'low-velocity' side, the 'blueshifted' and the 'redshifted' sides, where we included only the channels exhibiting line emission. The maxima are located at a velocity $v_{LSR} = 0.25$ km s$^{-1}$ with a mean intensity of 9.32 mJy beam$^{-1}$ for the blue part, $v_{LSR} = 4.78$ km s$^{-1}$ with a mean intensity of 6.89 mJy beam$^{-1}$ for the low velocity and $v_{LSR} = 7.50$ km s$^{-1}$ with mean intensity of 11.65 mJy beam$^{-1}$ for the redshifted side. In Table 2, we present a summary of the lines profile values.

The moments 0 maps of $^{12}$CO associated with the above velocity ranges are shown in Fig. 3 and a more detailed velocity channel map is shown in the online material.

The blueshifted side indicates that the gas approaching along the line of sight is concentrated in a massive shell that extends from the centre-west to the north-east of the image. The extended cavity goes from a distance of ∼1344 au (3.2 arcsec) from the centre of the disc to ∼4200 au (10 arcsec). The rms of the blueshifted moment 0 image is 60 mJy beam$^{-1}$ km s$^{-1}$.

The low-velocities channels show a diffuse and low flux emission distributed in the shape of a half-ring, centred in the bottom-left side of the image. The radius of the half-ring is ∼3000 au. The redshifted side shows a compact ring of strong emission, slightly decentered (∼600 au) from the disc position, with a radius of ∼1500 au.

### 3.3 $^{13}$CO moments

The $^{13}$CO has a lower optical depth with respect to the $^{12}$CO and it is a tracer of medium density material (∼$10^4$ cm$^{-3}$; Lequeux 2005). Similar to that of the $^{12}$CO emission, the intensity of the $^{13}$CO versus the velocity presents more than one peak. The plot of the line intensity versus velocity is displayed in Fig. 2. Similar to the case of $^{12}$CO data, we divided the data cube in two parts: the redshifted side and the blueshifted side. The maxima are located at $v_{LSR} = 1.75$ km s$^{-1}$ with a mean intensity of 3.36 mJy beam$^{-1}$ for the blue part and $v_{LSR} = 4.25$ km s$^{-1}$ with a mean intensity of 7.30 mJy beam$^{-1}$ for the redshifted part. The rms is 18.07 mJy beam$^{-1}$ km s$^{-1}$. The moment 0 map for the two sides are shown in Fig. 4 and a more detailed velocity channels map is shown in the online material.

The blueshifted part of the $^{13}$CO line is similar to that of the blue side of the $^{12}$CO emission. The gas is located in the same extended shell, as shown in Fig. 5 (left), where we overplotted with contour lines the emission of the $^{13}$CO on the blueshifted moment 0 map of the $^{12}$CO line. The redshifted part of the gas spatially coincides with the ring seen in the redshifted part of the $^{12}$COline, as shown in Fig. 5 (right), but with velocities comparable with the low-velocities side of the $^{12}$CO. This unusual behaviour has also been noticed in the outflow of the object HH 46/47 (Zhang et al. 2016). In fact, as we can see from the plot in Fig. 2, the two peaks of the $^{13}$CO emission are a scaled (in flux) version of the profile of the $^{12}$CO emission, with closer velocities to the systemic velocity. The distribution along the velocity axis is the same for both emission lines and the correspondent low-velocity side is apparently too weak to be detected.

When well mixed, $^{12}$CO and $^{13}$CO trace the same material. However, that does not mean that the emerging emission lines appear the same. This is due to an optical depth effect rather than a different density field. For example, in an outflow, at higher velocity, the column density of the material is not high and both the isotopologues are optically thin. In such a case, the $^{13}$CO emission may be too faint to be detected and we only see the outflow structure in the $^{12}$CO emission. At low velocities, the outflow material has

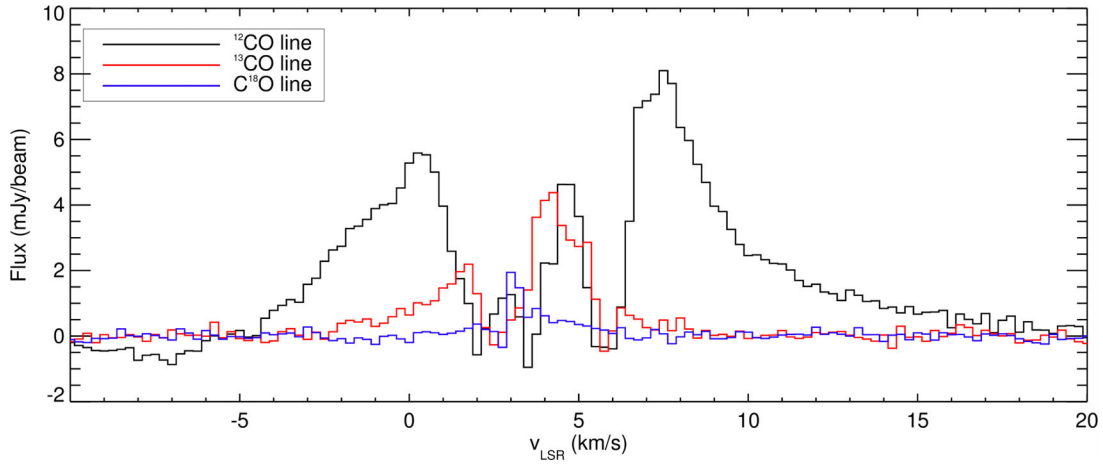


**Figure 2.** Plot showing the mean flux (inside the 19 arcsec circular region around the continuum) of the $^{12}$CO, $^{13}$CO and C$^{18}$O lines together versus the optical velocities. Three different peaks have been identified for the $^{12}$CO line: at $v_{LSR} = 0.25$, 4.78 and 7.50 km s$^{-1}$. Two different peaks have been identified for the $^{13}$CO line: at $v_{LSR} = 1.75$ and 4.25 km s$^{-1}$. The intensity of the C$^{18}$O line is significantly fainter than the other two lines, its maximum is found at $v_{LSR} = 3.0$ km s$^{-1}$.

**Table 2.** Added an entry to the table. Gas lines profiles. As the line profiles are asymmetric, we refer to the peak of the emission. The velocity $v_{LSR}$ and the mean flux at the peak of each side is indicated as $v_s$ and $F_s$, respectively.

| | Side | Range (km s$^{-1}$) | $v_s$ (km s$^{-1}$) | $F_s$ (mJy beam$^{-1}$) | $v_s - v_{C^{18}O}$ (km s$^{-1}$) |
|---|---|---|---|---|---|
| $^{12}$CO | B | $-5 \sim 2$ | 0.25 | 9.32 | $-2.85$ |
| | L | $4 \sim 5.25$ | 4.78 | 6.89 | 1.68 |
| | R | $6 \sim 16$ | 7.5 | 11.65 | 4.4 |
| $^{13}$CO | B | $-2.5 \sim 2.5$ | 1.75 | 3.36 | $-1.35$ |
| | R | $2.75 \sim 7.5$ | 4.25 | 7.30 | 1.15 |
| C$^{18}$O | L | $2.75 \sim 4$ | 3.1 | 1.94 | 0 |

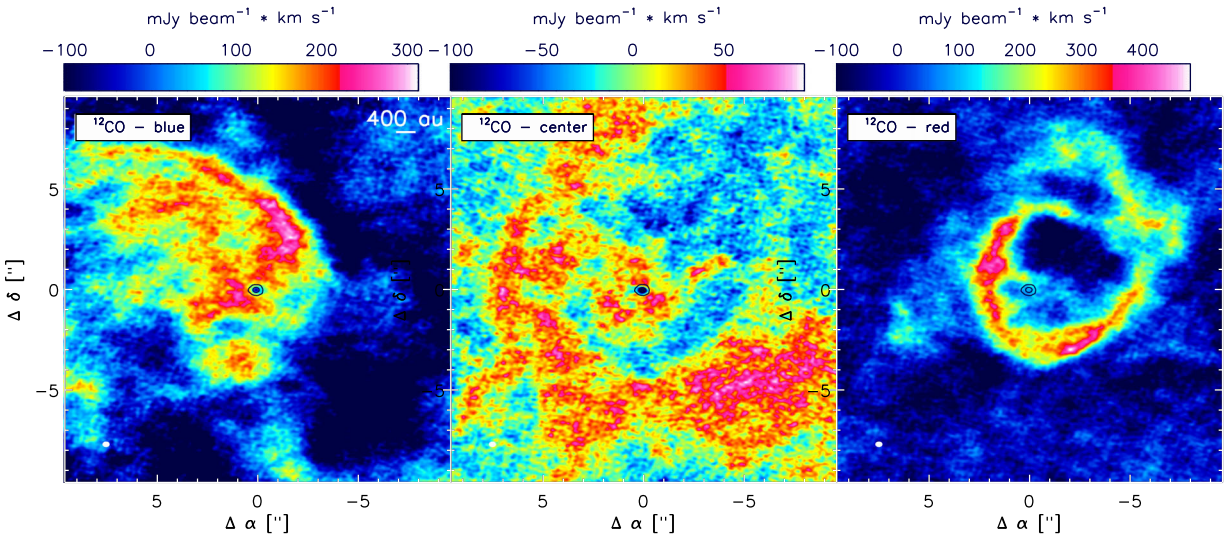


**Figure 3.** Moments 0 maps of the $^{12}$CO line. The blueshifted side of the velocities (left), the low-velocities side (centre) and the redshifted side (right) are shown. We divided the three parts following the velocity ranges listed in Table 2. The beam size is ∼0.25 arcsec, shown on the lower-left corner of the image. The continuum is shown in blue contour map.

much higher column density and it starts to mix up with the cloud material. For optically thin tracers like $^{13}$CO, outflow structure can still be distinguished from the cloud emission because the outflow material piled up along the outflow cavity with higher column density. In the case of interferometric observation, the cloud emission may be completely filtered out and only the outflow cavities are seen. Meanwhile, $^{12}$CO quickly becomes optically thick at these velocities, therefore it is hard to distinguish outflow emission from

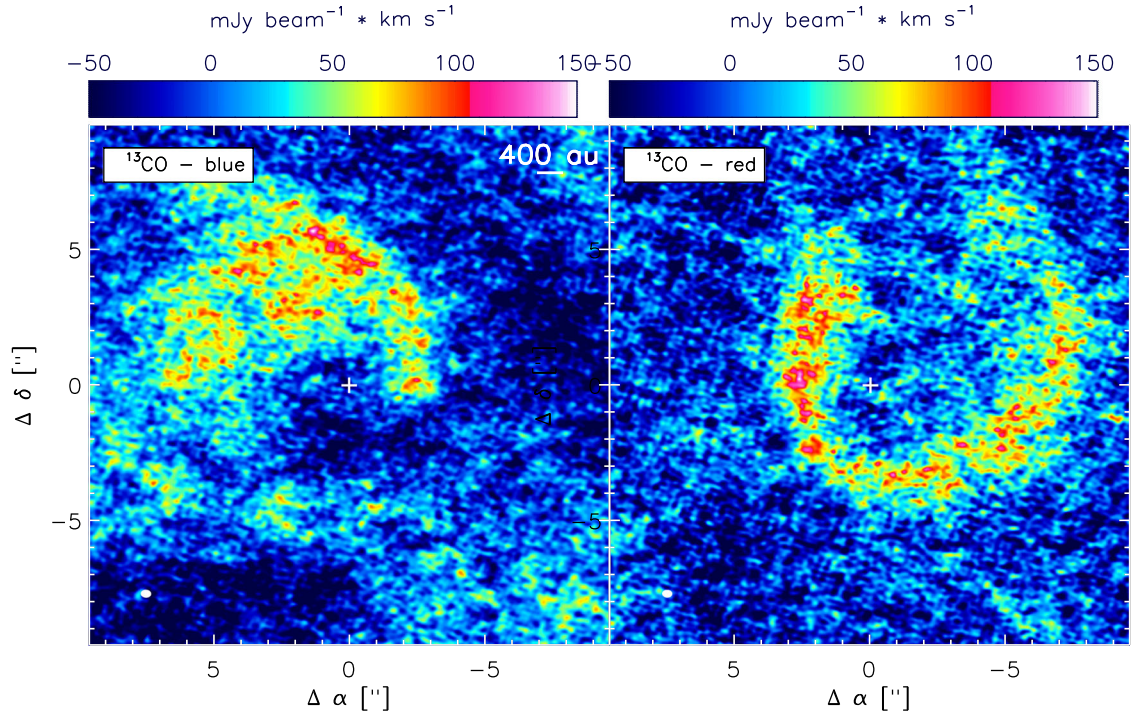


**Figure 4.** Moments 0 maps of the $^{13}$CO line. The blueshifted side (left) and the redshifted part (right) are shown. The velocity ranges are listed in Table 2 and the beam size is ∼0.25 arcsec, which is shown in the lower-left corner of the images. The position of the continuum emission is indicated as a white cross.

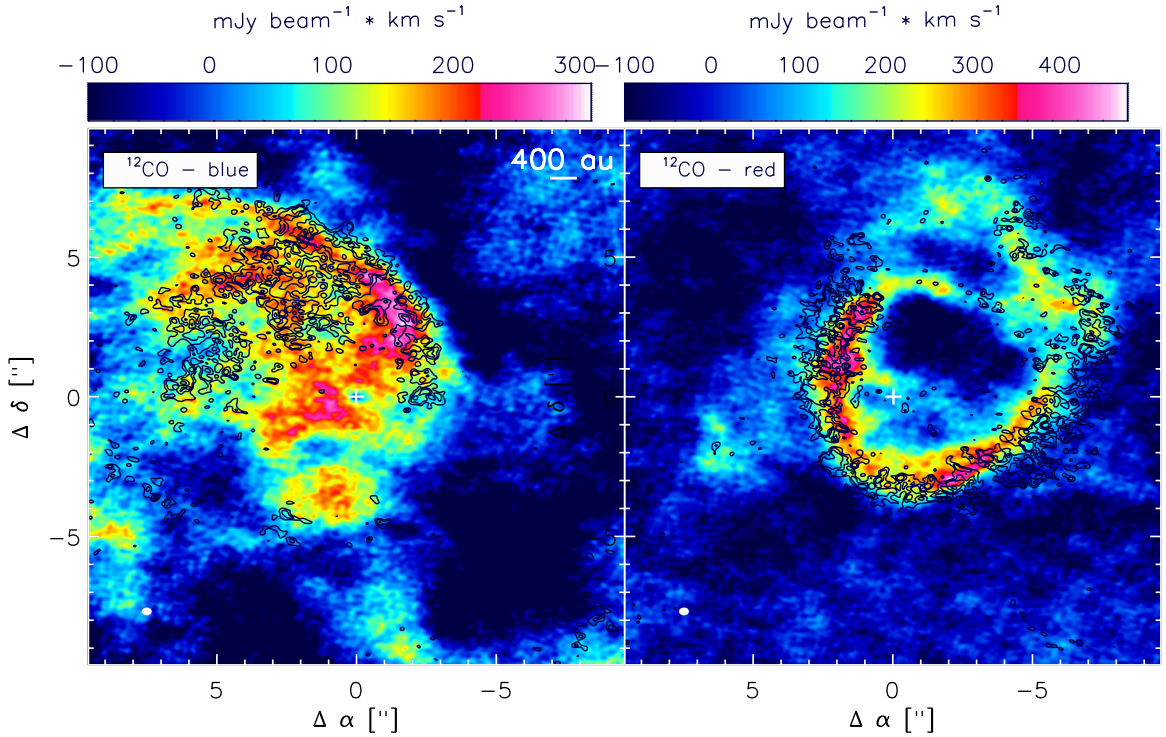


**Figure 5.** Left: image showing the blueshifted side of the $^{12}$CO line with the black contour map of the blueshifted side of the $^{13}$CO line. Both tracers are located in the same shell. The continuum is shown as a white cross. Right: image showing the redshifted side of the $^{12}$CO line with the black contour map of the redshifted side of the $^{13}$CO line. Both tracers are located in the ring. The star is located on the position of the white cross. The beam size is ∼0.25 arcsec, shown on the lower-left corner of the image.

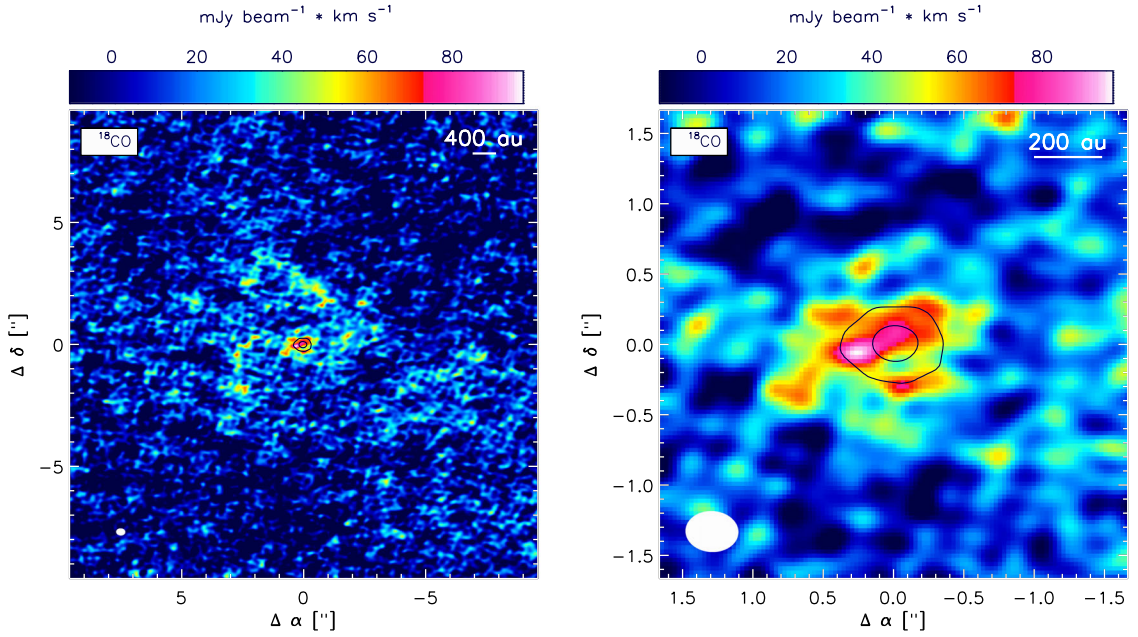


**Figure 6.** Moment 0 map of the $C^{18}O$ line. On the right-hand side, a zoom around the centre of the disc is shown. The beam size is ∼0.25 arcsec, shown on the lower-left corner of the image. The continuum is shown as blue contours.

the cloud emission. In the case of our observations, the maximum angular scale is 11.4 arcsec and the cloud emission may be filtered out.

The $^{12}$CO shows absorption in some places where the $^{13}$CO peaks, suggesting multiple cones/rings along the line of sight with an ordered velocity gradient.

### 3.4 $C^{18}O$ moments

The $C^{18}O$ emission is found in one peak of the intensity versus velocities plot, corresponding to the low velocities of the $^{12}$CO. The rms is 10.79 mJy beam$^{-1}$ km s$^{-1}$. The moment 0 map for the $C^{18}O$ line is shown in Fig. 6. The emission of this line is significantly fainter with respect to the lines of the $^{12}$CO and $^{13}$CO, as we show in Fig. 2. The emission peaks at the location of the disc, as indicated via the continuum emission and the spectrum is narrow, consistent with the low inclination of ∼14° from the continuum fitting.

### 3.5 Disc gas mass estimate

The strong $^{12}$CO and $^{13}$CO emission indicates extended structure related to the protostellar outburst and its effect on the surrounding envelope. Fig. 2 shows strong absorption from this envelope and this precludes a detection of these lines in the disc. The $C^{18}O$ line also shows some extended emission but the absorption is much weaker due to its lower optical depth and we find a compact source centred on the continuum source. The flux of this compact source is 0.15 Jy km s$^{-1}$. The value of the dust temperature is set as 20 K. The gas temperature is a parametric function of radius and vertical height above the mid-plane. We use this to estimate a lower limit to the disc gas mass of 3 $M_{\rm Jup}$ based on the models of Williams & Best (2014).

The gas mass may be considerably higher if the disc is so cold that most of the gas is below 20 K and the CO is frozen out. The dust mass is estimated to be $\sim 1.6 \times 10^{-3}\, M_{\odot}$ for 'standard' dust opacity, $\kappa = 2.2\,{\rm cm^2\,g^{-1}}$ and temperature, $T_{\rm dust} = 20$ K (e.g. Williams & Cieza 2011). Therefore, even if the gas mass is underestimated by an order of magnitude, the gas-to-dust ratio appears to be much lower than the interstellar medium ratio of 100. Williams & Best (2014) and Ansdell et al. (2016) also found very low CO isotopologue line-to-continuum ratios in Taurus and Lupus discs. If we assume the typical gas-to-dust ratio of ∼20 measured in Taurus and Lupus discs, based on [$^{13}$CO/$C^{18}O$] compared to the continuum, the gas mass would be ∼30 $M_{\rm Jup}$. Our finding here suggests the loss of gas or chemical effect that creates such a low $C^{18}O$ line to continuum ratio, which is very rapid and perhaps may be related to the strong outbursts of early protostellar evolution.

Indeed, comparing our results with the archetype of the EXor class, EX Lup, Banzatti et al. (2015) found that after the strong outburst of 2008, the CO decreased dramatically. This can be caused by a rapid depletion of gas accumulated beyond the disc corotation radius during quiescent periods. Kóspál et al. (2016) found that EX Lup has a modest CO depletion. Using the $^{13}$CO line and the canonical $10^{-4}$ CO-to-$H_2$ abundance ratio, they estimate a total disc mass of $2.3 \times 10^{-4}$ $M_{\odot}$. This results can be a factor of 10–100 lower than the actual value taking into account the CO depletion.

### 3.6 Outflow gas parameters

Column density, mass, momentum and kinetic energy of the expanding gas are listed in Table 3. To calculate these quantities, we used the formalism presented in Perez et al. (2015) and applied it to both the $^{12}$CO and $^{13}$CO isotopologues. We did not determine these properties for the $C^{18}O$ gas because its emission was too weak. The correction for the optical depth (see e.g. Dunham et al. 2014) cannot be applied for this data set, as only a few velocity channels present emission from both the isotopologues. The values presented are then lower limits of these quantities. We adopt in this paper an abundance of the $^{12}$CO relative to $H_2$ of $10^{-4}$ and a relative abundance between $^{12}$CO and $^{13}$CO of 62 (Langer & Penzias 1993). The excitation temperature, assumed constant along the line of sight, has a value of $T_{\rm ex} = 50$ K in this analysis. The beam filling factor is assumed to be 1. The total mass of the gas is defined as $M = \sum_v {\rm M}(x,y,v)$, the

**Table 3.** Column density, mass, momentum and kinetic energy of the outflow.

| Molecule | Side | Column density ($10^{20}$ m$^{-2}$) | Mass ($10^{-3}$M$_\odot$) | Momentum ($10^{-3}$M$_\odot$ km s$^{-1}$) | Energy ($10^{40}$ erg) |
|---|---|---|---|---|---|
| $^{12}$CO | Blueshifted | 2.8 | 1.8 | 6.9 | 29 |
| | Redshifted | 6.2 | 10.5 | 53 | 280 |
| | Total | 9.0 | 12.3 | 60.0 | 310 |
| $^{13}$CO | Blueshifted | 0.7 | 0.2 | 0.3 | 0.8 |
| | Redshifted | 1.3 | 1.0 | 1.3 | 2.0 |
| | Total | 2.0 | 1.1 | 1.6 | 2.8 |

momentum surface density is defined as $P = \sum_v \mathrm{M}(x,y,v)v$ and the kinetic energy surface density as $E = \sum_v \mathrm{M}(x,y,v)v^2/2$, where $v = v_{\mathrm{LSR}} - v_{\mathrm{C^{18}O}}$ and $\mathrm{M}(x,y,v)$ is the mass surface density calculated for each velocity channel.

The values found for our object have the same order of magnitude of other protostars presented in literature: for example, Arce & Sargent (2006) presented observations of nine low-mass, Class 0, I and II sources with detected outflows. They found outflows' masses in the range of 6–150 $\times$ $10^{-3}$ M$_\odot$, with momenta in the range 4–119 $\times$ $10^{-3}$ M$_\odot$ km s$^{-1}$ and kinetic energy of 2–484 $\times$ $10^{40}$ erg. These values are very similar to those reported here for V2775 Ori, keeping in mind that this source is seen face-on, so only a small portion of the outflow is detected. Similar values are found for HL Tau system (Klaassen et al. 2016).

Due to the inclination of the outflow, we cannot estimate the size of the outflow along the $z$-axis (towards us) and consequently the age of the system. We can speculate that the component of the velocity of the gas along the plane of the sky should be lower than the component along the $z$-axis; as Arce & Sargent (2006) suggest, young Class 0 object have highly collimated outflows. If this is the case, taking the highest velocity of the gas, i.e. 4.5 km s$^{-1}$ for the redshifted part and assuming it constant and the radius of the ring of 1500 au, the kinetic age of the outflow would be less than $\sim$1600 yr. Another independent way to estimate the age of the outburst is to assume that the axis of the hourglass is normal to the plane of the disc, which is inclined by $\sim$14°. Taking into account that the centre of the redshifted ring is shifted by 600 au, the hourglass half-axis would be of 2500 au. In this case, the opening angle of the outflow is of 30° and the age is about 2600 yr. As the disc is almost face-on, the uncertainties on these values are high. Nevertheless, the same order of magnitude is found for HL Tau (2600 yr; Klaassen et al. 2016) and HBC 494 (2900 yr; Ruíz-Rodríguez 2016). The outflow of V2775 Ori is much more collimated than the one of HBC 494 ($\sim$150°; Ruíz-Rodríguez 2016). Arce & Sargent (2006) suggest that there is a correlation between the opening angle of the outflow and the age of the system: the opening angle is increasing for more evolved system. The age of 0.1 Myr for V2775 Ori is compatible with the value of the opening angle of 30°.

## 4 DISCUSSION

The $^{12}$CO emission traces cool material and it is optically thick. The emission measured of this line presents three peaks for this FUor object: one in the blueshifted side of the velocities, one in the low-velocities side and one in the redshifted velocities. This indicates that the gas is expanding from the disc and as it is seen face-on, we expect to look through the outflow of this object. Indeed, in the blue and red sides of the velocities, the gas is located in circular shapes and aligned with respect to the disc (Fig. 7). That means that the axis of the 'hourglass' shape is almost aligned with the line of sight. A cartoon sketch of the system is presented in Fig. 8. On the

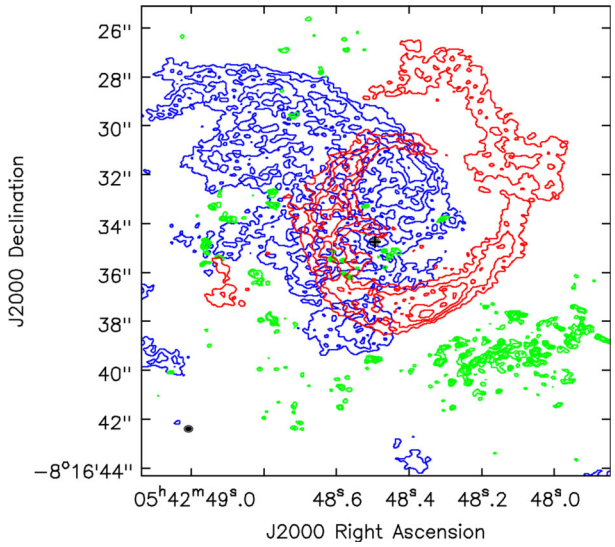


**Figure 7.** Three colours to simulate a 3D image showing the blueshifted, central and red-shifted part of the $^{12}$CO line emission. The three different zones are shown in blue, green and red contours for the blueshifted, low velocities and redshifted parts respectively. The contours represent 0.2, 0.4, 0.6, 0.8 step levels of 0.04 Jy beam$^{-1}$. The continuum emission is located where the black cross is. The beam size is $\sim$0.25 arcsec, shown on the lower-left corner of the image. A cartoon representation can be found in Fig. 8.

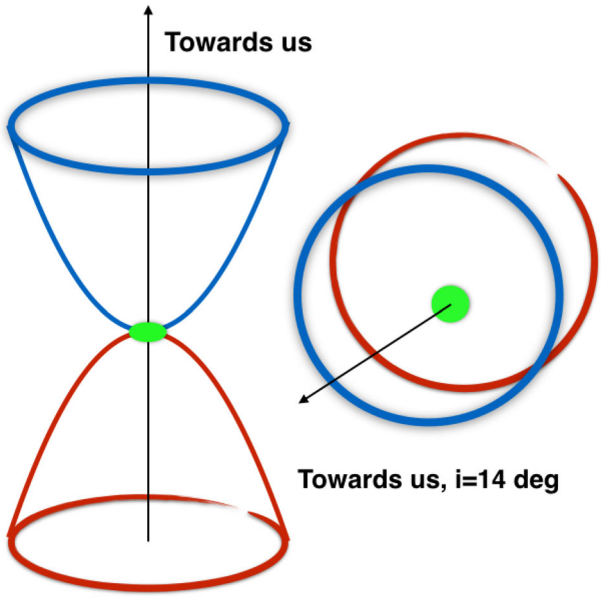


**Figure 8.** Cartoon sketch of the system V2775 Ori. The palette of colours is the same of Fig. 7 to indicate different regions of the outflow. The disc is not to scale. The arrows indicate the axis of the hourglass.

other hand, we do not see the walls of this hourglass. The emission is concentrated in the shell (approaching us) and the ring shape (moving away from us) but there is almost no connection between these regions and the disc. The last outburst for this object took place between 2005 and 2007. If we assume a constant velocity for the gas of 5 km $s^{-1}$ (Klaassen et al. 2016), the ejected gas should be located at ∼12 au away from the star by now. The outburst seen in our data set cannot be that close to the star, which suggests that the $^{12}$CO is a remnant left from a previous outflow ∼2000 yr old, given the dynamical age estimated in the previous section. The shells apparent in the data represent cavities in the molecular cloud excavated by the outflow of the FUor. This scenario is similar to the one presented by Quillen et al. (2005), where they speculate that the cavities seen in the molecular cloud NGC 1333 are the fossils of ancient outflows of pre-main-sequence stars.

Since accretion and outflow rates are intimately connected, an episodic outflow scenario is perfectly consistent with the episodic accretion paradigm (Audard et al. 2014). In fact, clear signatures of such episodic molecular outflows have recently been imaged by ALMA (Plunkett et al. 2015).

In our object, the blueshifted emission of the $^{13}$CO line is located at the same position of the blueshifted part of the $^{12}$CO, same for the redshifted part but with velocities comparable to the low-velocities side of the $^{12}$CO. We can interpret this phenomenon as emission from the $^{12}$CO and $^{13}$CO lines tracing the low- and medium-density gas, respectively. Then, the $^{13}$CO is moving with lower velocities because of the higher density of the gas that it is tracing. Again, in this emission line, we do not see the walls of the cone-shape outflow but only two symmetrical circular features, expanding away from the disc.

The C$^{18}$O is optically thin and thus probes deeper regions. Plunkett et al. (2015) suggest that the C$^{18}$O may trace the envelope of the circum-stellar disc. We detected very faint gas emission from the disc of V2775 Ori and we use this to estimate the velocity of the system. If we assume that the velocity of the C$^{18}$O is the velocity of the system, we can estimate that the blue-side emission of the $^{12}$CO line is approaching us with a velocity of 2.85 km $s^{-1}$, while the red side is expanding away from us with a velocity of 4.4 km $s^{-1}$ (see Table 2). The non-symmetrical velocities may be explained by the fact that the gas is expanding into a space with material of different densities. Similar velocities but slightly lower are found for the outflow of HBC 494 (Ruíz-Rodríguez et al. 2016). The higher density gas traced by the $^{13}$CO is moving slower with symmetric velocities of ∼1 km $s^{-1}$.

## 5 SUMMARY

We observed the FUor object V2775 Ori with ALMA and obtained a resolved image of the disc continuum emission with a resolution of 0.25 arcsec. The disc is seen nearly face-on, with an inclination of ∼14°. The characteristic radius of the disc is ∼30 au. We also obtained three narrow bands centred on the $^{12}$CO(2–1, 230.5 GHz) line, the $^{13}$CO (2–1, 220.4 GHz) line and the C$^{18}$O (2–1, 219.6 GHz) line. The $^{12}$CO and $^{13}$CO emission features show similar structures expanding from the disc: the blueshifted side of the gas is concentrated in an extended shell, while the redshifted side is concentrated in a compact ring. The denser gas, traced by $^{13}$CO emission, is moving with lower velocities with respect to the $^{12}$CO, but is tracing the same structures. Since we cannot see the walls of this 'hourglass', we can interpret these structures as cavities created by an ancient outflow. We argue that this structure is a fossil of an outburst occurring before the previous outburst in 2005–2007. Similar cavities have been already seen in other molecular clouds (see e.g. Quillen et al. 2005). The previous outburst, assuming than the outflow is collimated (i.e. with an opening angle < 45°), had occurred less than 1600 yr ago. The opening angle of the outburst should be of the order of 30°, given the decentered position of the redshifted ring of the $^{12}$CO.

## ACKNOWLEDGEMENTS

This paper is based on Atacama Large Millimeter/submillimiter Array (ALMA) observations, program number 2013.1.00710.S. It makes use of the following ALMA data: ADS/JAO.ALMA#2013.1.00710.S. ALMA is a partnership of ESO (representing its member states), NSF (USA) and NINS (Japan), together with NRC (Canada), NSC and ASIAA (Taiwan) and KASI (Republic of Korea), in cooperation with the Republic of Chile. The Joint ALMA Observatory is operated by ESO, AUI/NRAO and NAOJ. The National Radio Astronomy Observatory is a facility of the National Science Foundation operated under cooperative agreement by Associated Universities, Inc. AZ and LAC acknowledge support from the Millennium Science Initiative (Chilean Ministry of Economy) through grant 'Nucleus RC130007'. LAC also acknowledges support from FONDECYT-CONICYT grant #1140109. HC acknowledges support from the Spanish Ministerio de Economía y Competitividad under grant AYA2014-55840P. SP acknowledges financial support by FONDECYT grant #3140601. DAP acknowledges FONDECYT grant #3150550.

## REFERENCES

Andrews S. M., Williams J. P., 2005, ApJ, 631, 1134
Ansdell M. et al., 2016, ApJ, 828, 46
Arce H. G., Sargent A. I., 2006, ApJ, 646, 1070
Armitage P. J., Livio M., Pringle J. E., 2001, MNRAS, 324, 705
Audard M. et al., 2014, in Beuther H., Klessen R. S., Dullemond C. P., Henning T., eds, Protostars and Planets VI. Univ. Arizona Press, Tucson, AZ, p. 387
Banzatti A., Pontoppidan K. M., Bruderer S., Muzerolle J., Meyer M. R., 2015, ApJ, 798, L16
Bell K. R., Lin D. N. C., 1994, ApJ, 427, 987
Bonnell I., Bastien P., 1992, ApJ, 401, L31
Caratti o Garatti A. et al., 2011, A&A, 526, L1
Cieza L. A. et al., 2016, Nature, 535, 258
Cutri R. M. et al., 2003, The IRSA 2MASS All-Sky Point Source Catalog, NASA/IPAC Infrared Science Archive. Available at: http://irsa.ipac.caltech.edu/applications/Gator/
Dunham M. M., Arce H. G., Mardones D., Lee J.-E., Matthews B. C., Stutz A. M., Williams J. P., 2014, ApJ, 783, 29
Evans II N. J., Balkum S., Levreault R. M., Hartmann L., Kenyon S., 1994, ApJ, 424, 793
Fischer W. J. et al., 2012, ApJ, 756, 99
Gramajo L. V., Rodón J. A., Gómez M., 2014, AJ, 147, 140
Hales A. S., Corder S. A., Dent W. R. D., Andrews S. M., Eisner J. A., Cieza L. A., 2015, ApJ, 812, 134
Hartmann L., Kenyon S. J., 1985, ApJ, 299, 462
Hartmann L., Kenyon S. J., 1996, ARA&A, 34, 207
Henning T., Burkert A., Launhardt R., Leinert C., Stecklum B., 1998, A&A, 336, 565
Herbig G. H., 1966, Vistas Astron., 8, 109
Klaassen P. D., Mottram J. C., Maud L. T., Juhasz A., 2016, MNRAS, 460, 627
Kóspál Á., 2011, A&A, 535, A125
Kóspál Á. et al., 2016, ApJ, 821, L4
Langer W. D., Penzias A. A., 1993, ApJ, 408, 539

Lequeux J., 2005, The Interstellar Medium. Astronomy and astrophysics library, Springer, Berlin
Lodato G., Clarke C. J., 2004, MNRAS, 353, 841
McMullin J. P., Waters B., Schiebel D., Young W., Golap K., 2007, in Shaw R. A., Hill F., Bell D. J., eds, ASP Conf. Ser. Vol. 376, Astronomical Data Analysis Software and Systems XVI. Astron. Soc. Pac., San Francisco, p. 127
Menten K. M., Reid M. J., Forbrich J., Brunthaler A., 2007, A&A, 474, 515
Perez S. et al., 2015, ApJ, 798, 85
Plunkett A. L., Arce H. G., Mardones D., van Dokkum P., Dunham M. M., Fernández-López M., Gallardo J., Corder S. A., 2015, Nature, 527, 70
Quillen A. C., Thorndike S. L., Cunningham A., Frank A., Gutermuth R. A., Blackman E. G., Pipher J. L., Ridge N., 2005, ApJ, 632, 941
Ruíz-Rodríguez D. et al., 2016, MNRAS, in press
Sandell G., Weintraub D. A., 2001, ApJS, 134, 115
Vorobyov E. I., Basu S., 2005, ApJ, 633, L137
Williams J. P., Best W. M. J., 2014, ApJ, 788, 59
Williams J. P., Cieza L. A., 2011, ARA&A, 49, 67
Zhang Y. et al., 2016, ApJ, preprint (arXiv:1602.02388)
Zhu Z., Hartmann L., Gammie C., McKinney J. C., 2009, ApJ, 701, 620
Zhu Z., Hartmann L., Nelson R. P., Gammie C. F., 2012, ApJ, 746, 110

## SUPPORTING INFORMATION

Supplementary data are available at *MNRAS* online.

**suppl_data**

Please note: Oxford University Press is not responsible for the content or functionality of any supporting materials supplied by the authors. Any queries (other than missing material) should be directed to the corresponding author for the article.

This paper has been typeset from a TEX/LATEX file prepared by the author.